

Facile preparation of graphene oxide/Poly (N-Isopropylacrylamide-co-acrylic acid) composite thin film and its quartz crystal microbalance humidity sensing property

Journal of Polymer Science

Ji, Le; Pan, Yuran; Cao, Zheng; Wang, Ruotong; Yang, Haicun et al

<https://doi.org/10.1002/pol.20240504>

This publication is made publicly available in the institutional repository of Wageningen University and Research, under the terms of article 25fa of the Dutch Copyright Act, also known as the Amendment Taverne.

Article 25fa states that the author of a short scientific work funded either wholly or partially by Dutch public funds is entitled to make that work publicly available for no consideration following a reasonable period of time after the work was first published, provided that clear reference is made to the source of the first publication of the work.


This publication is distributed using the principles as determined in the Association of Universities in the Netherlands (VSNU) 'Article 25fa implementation' project. According to these principles research outputs of researchers employed by Dutch Universities that comply with the legal requirements of Article 25fa of the Dutch Copyright Act are distributed online and free of cost or other barriers in institutional repositories. Research outputs are distributed six months after their first online publication in the original published version and with proper attribution to the source of the original publication.

You are permitted to download and use the publication for personal purposes. All rights remain with the author(s) and / or copyright owner(s) of this work. Any use of the publication or parts of it other than authorised under article 25fa of the Dutch Copyright act is prohibited. Wageningen University & Research and the author(s) of this publication shall not be held responsible or liable for any damages resulting from your (re)use of this publication.

For questions regarding the public availability of this publication please contact openaccess.library@wur.nl

RESEARCH ARTICLE

Facile preparation of graphene oxide/Poly(*N*-Isopropylacrylamide-co-acrylic acid) composite thin film and its quartz crystal microbalance humidity sensing property

Le Ji¹ | Yuran Pan¹ | Zheng Cao^{1,2}  | Ruotong Wang¹ | Haicun Yang¹ | Junfeng Cheng¹ | Chunlin Liu^{1,2} | Xiaowang Lu³ | Louis C. P. M. de Smet⁴

¹Jiangsu Key Laboratory of Environmentally Friendly Polymeric Materials, School of Materials Science and Engineering, Jiangsu Collaborative Innovation Center of Photovoltaic Science and Engineering, Changzhou University, Changzhou, Jiangsu, People's Republic of China

²Department of Mechanical and Materials Engineering, Changzhou University Huaide College, Jingjiang, People's Republic of China

³School of Material Science and Engineering, Yancheng Institute of Technology, Yancheng, People's Republic of China

⁴Advanced Interfaces & Materials, Laboratory of Organic Chemistry, Wageningen University, Wageningen, The Netherlands

Correspondence

Zheng Cao and Haicun Yang, Jiangsu Key Laboratory of Environmentally Friendly Polymeric Materials, School of Materials Science and Engineering, Jiangsu Collaborative Innovation Center of Photovoltaic Science and Engineering, Changzhou University, Changzhou 213164, Jiangsu, People's Republic of China.
Email: zcao@cczu.edu.cn and yhcobo@cczu.edu.cn

Funding information

National Natural Science Foundation of China, Grant/Award Number: 21704008; Postgraduate Research & Practice Innovation Program of Jiangsu Province, Grant/Award Number: KYCX23_3036

Abstract

The composite microgels were synthesized from *N*-Isopropylacrylamide (NIPAM) and acrylic acid (AA) monomers in the presence of graphene oxide (GO) using an in situ radical copolymerization method. The successful preparation of these composite microgels was investigated through Fourier transform infrared spectroscopy (FTIR), ultraviolet visible absorption spectroscopy (UV-vis), and Raman spectroscopy. Due to the hydrophilic properties of GO and the microgels containing oxygenated groups (—OH, —COOH, and —CONH₂), quartz crystal microbalance (QCM) sensors can be fabricated by spraying the GO/P(NIPAM-co-AA) dispersion onto QCM sensors as sensitive coating materials. The results indicate a notable enhancement in the performance of GO/P(NIPAM-co-AA) modified QCM humidity sensor, compared to QCM sensors modified with either GO or P(NIPAM-co-AA) microgels alone. This improvement is mainly evidenced by higher sensitivity and reduced moisture hysteresis. The humidity sensing mechanism is based on the combined effect of GO and P(NIPAM-co-AA) microgels, which synergistically enhance the sensor's performance. Additionally, the results from water contact angle measurements, laser scanning confocal microscopy (LSCM), and scanning electron microscope (SEM) show that GO/P(NIPAM-co-AA) exhibits greater roughness and stronger hydrophilicity than either GO or P(NIPAM-co-AA) microgels alone. These properties make GO/P(NIPAM-co-AA) an effective moisture-sensitive material for QCM sensors.

KEYWORDS

graphene oxide, humidity, microgels, QCM, sensor

1 | INTRODUCTION

With the advancement of technology, people are experiencing the Fourth Industrial Revolution, characterized by intelligent products and the Internet of Things (IoT). This revolution places higher demands on sensors, which are essential for collecting, processing, and interacting with information.¹ A sensor typically consists of a sensitive device, a signal conversion system, and a data receiving and processing system, enabling the conversion of the measured information into a visual signal for output. Depending on their sensing targets, sensors can be categorized into various types, including pressure, temperature, humidity, and optical sensors.^{2–4}

Changes in humidity are closely related to human activity and have significant impacts in many fields, and the effective humidity detection methods are therefore crucial. For instance, in industrial manufacturing, humidity directly affects the normal operation of precision instruments and circuits, as well as the lifespan of production equipment. In agriculture, soil moisture levels directly impact the healthy growth of crop roots and the maintenance of dynamic water balance. In drug storage, excessive humidity can lead to drug hydrolysis, mold growth, and reduced efficacy. Regarding human health, the humidity of exhaled air, which is approximately 90% relative humidity (RH), can be used to monitor a patient's breathing in real-time, as the frequency of breathing varies in different states. Given the diverse and complex requirements for humidity detection in industrial production and daily life, there is an urgent need for a humidity sensor that offers fast response times, high stability, and other excellent humidity-sensitive characteristics.

Humidity sensors typically consist of humidity-sensitive components, signal conversion systems, and data reception and processing systems. The sensing principle is that the humidity-sensitive material on the humidity-sensitive element adsorbs different amounts of water molecules through physical or chemical interactions in various humidity environments. This adsorption changes the sensor's relevant signal, reflecting the humidity change as a signal variation and achieving the purpose of sensing. According to the different sensing signals, commonly studied humidity sensors include resistive sensors,^{5–7} capacitive sensors,^{8–10} colorimetric sensors,^{11–13} strain sensors,^{14,15} capacitive micromachined ultrasonic transducer (CMUT) sensors,^{16,17} and quartz crystal microbalance (QCM) sensors.^{18,19}

QCM sensors have very high sensitivity, capable of detecting changes in nanogram mass, and are widely used in protein adsorption,²⁰ antipollution materials,²¹ sensors,^{22,23} and surface-interface interaction research.^{24–26} However, a QCM sensor itself does not have selectivity or adsorption for

the detection molecules, relying mainly on the corresponding sensitive layer loaded on its surface to adsorb the detection molecules and achieve the purpose of sensing. For QCM-based humidity sensors, humidity-sensitive materials are key to effective detection and must meet inspection requirements, such as stability and repeatability. In existing literature, the moisture-sensitive materials used for QCM humidity sensors mainly include carbon materials,^{27,28} two-dimensional materials,²⁹ metal oxide materials,^{30,31} and polymer materials.^{6,32} For example, Su and Xie et al. have carried out extensive work on preparation of various nanomaterials including, piezoelectric composite,^{33,34} zinc oxide nanorods,³⁵ gas sensor array,³⁶ core-shell structured smart textiles,³⁷ and biodegradable cotton fiber-based piezoresistive textiles,³⁸ and establishment of sensors for the detection of ammonia, humidity, NH₃, NO₂, and human biomechanical activity, respectively. Qi et al.³⁹ prepared polydopamine (PDA) films on QCM sensors using in-situ growth method. The results showed that the PDA-QCM humidity sensor with 2 h polymerization growth time owned high sensitivity (20.77 Hz/% RH), good selectivity, short response/recovery time (5 s/11 s), and acceptable long-term stability. Yuan et al.⁴⁰ deposited a composite film based on graphene oxide (GO) and polyethylenimine (PEI) on the QCM sensor by a facile spray method. They obtained high sensitivity (27.25 Hz/%RH), low hysteresis (0.54%RH) and short response/recovery time (<53 s/18 s). Cha et al.³⁰ prepared QCM transducers based on superhydrophilic ZnO nanoneedle array by a convenient and quick chemical deposition method. The sensors exhibit high sensitivity (21.4 Hz/%RH), fast response (2 s/2 s) and narrow hysteresis (maximum 2%RH), which is determined by the morphology and the wetting performance of nano-ZnO materials. There are still some minor problems with current methods, such as chemical synthesis, use of special reagents, complex routes, and cost issues. It is difficult to fully meet the performance requirements of moisture-sensitive materials by using a single inorganic nanomaterial or organic polymer material. Each type of moisture-sensitive material has its own advantages, and the design and selection of suitable coating material are essential to develop the reliable sensors based on QCM. The combination of materials with different advantages in a convenient way is the key to solving the above problems.

The two-dimensional (2D) material is rich in numerous hydrophilic functional groups, making it an ideal candidate for humidity sensors.^{41,42} Leng et al.⁴³ prepared a humidity sensor by self-assembling GO with polymers, and the results showed that the stability and linearity of the humidity sensor were both improved and enhanced. Ding et al.⁴⁴ developed a fullerene (C₆₀)/GO nanocomposite-based QCM sensor, which demonstrated superior performance, compared with

sensors using GO as sensing film. GO itself, as a 2D material, is easy to spread and possesses relatively good rigidity and hydrophilicity due to its edge oxygen-containing groups. However, GO generally needs to be combined with other functional materials to enhance the response performance and stability of the film on QCM sensors.⁴⁵

Microgels are one kind of cross-linked polymer particles.^{46–48} Through free radical copolymerization, monomers with various functional groups can be combined to endow the microgels with rich functionalities, such as $-\text{COOH}$, $-\text{NH}_2$, $-\text{CONH}-$, and $-\text{OH}$.⁴⁹ Microgels with tunable sizes and environmental responsiveness have found many applications in medical carrier,⁵⁰ catalysis,^{51,52} and sensors.⁵³ The interactions between microgel materials and dye molecules,⁵⁴ ions,^{55–57} and proteins⁵⁸ have also been extensively studied. When used as a moisture-sensitive material for QCM sensors, soft and wet microgels exhibit strong viscoelasticity and are prone to energy dissipation.⁵⁴ In contrast, GO is an inorganic and rigid material that can be combined with microgels to prepare composites suitable for QCM moisture sensing applications. We synthesized functional GO composite microgels by a free radical polymerization and fabricated the composite thin films by spraying the GO/P(NIPAM-co-AA) dispersion onto QCM sensors, which are responsive under varying relative humidity conditions, and suitable for the fabrication of QCM humidity sensors. We systematically studied the response of QCM sensor in the range of 11%–95% RH and investigated its response sensitivity, reversibility, repeatability, hysteresis characteristics, and long-term stability.

2 | MATERIALS AND METHODS

2.1 | Materials

N-Isopropylacrylamide (NIPAM, $\geq 98\%$), acrylic acid (AA, $\geq 99\%$), *N,N'*-methylenebisacrylamide (MBA, $\geq 99\%$), and potassium persulfate (KPS, $\text{K}_2\text{S}_2\text{O}_8$, $\geq 99\%$) were purchased from Beijing J&K Technology Co., Ltd. GO ($\geq 99\%$, 1–2 μm) was obtained from Nanjing Xianfeng Nanomaterial Technology Co., Ltd., China. Lithium chloride (LiCl), magnesium nitrate ($\text{Mg}(\text{NO}_3)_2$), sodium chloride (NaCl), magnesium chloride (MgCl_2), and potassium nitrate (KNO_3), all of analytical grade, were purchased from Sinopharm Reagent Co., Ltd.

2.2 | Microgel preparation

The GO composite microgel was synthesized using an in-situ free radical copolymerization method. MBA served as the crosslinker, while KPS was employed as the

initiator. Specifically, 0.9 g of NIPAM (8 mmol), 0.1 g of AA (2 mmol), and 0.06 g of MBA were added in 95 mL of deionized water. The mixture was stirred continuously at 400 rpm until it became a transparent solution. Nitrogen gas (N_2) was introduced for 0.5 h to eliminate oxygen from the system, following which the reaction solution was heated to 70 °C. Under identical experimental conditions, after 1 h, 2 mL of GO dispersion (2 mg/mL) and 5 mL of KPS solution (4 mg/mL) were introduced to initiate the copolymerization of NIPAM and AA. Observation revealed that after 6 h of reaction, the emulsion's color transitioned from light to dark brown, indicating the formation of the final product, the GO composite microgel with 0.4 wt% GO. Subsequently, the composite microgel underwent purification by dialysis to eliminate any unreacted molecules. By changing the concentration of GO dispersion, GO composite microgels with different GO content (0.2 wt%, 0.4 wt%, 0.6 wt%, and 0.8 wt%) can be obtained. The impact of supplementing GO content on the performance of QCM humidity sensors has been studied and can better explain the humidity sensing mechanism. For comparative analysis, pure P(NIPAM-co-AA) microgels were also prepared using the same process without adding GO.

2.3 | Construction of thin film

Figure 1 depicts the construction of the QCM sensor modified with a GO/P(NIPAM-co-AA) sensitive film. Initially, GO/P(NIPAM-co-AA) composite microgel suspension was evenly sprayed onto the surface of either a silicon wafer or a QCM sensor using an air spraying technique. The QCM sensors used were soaked in a piranha solution with strong oxidizing properties (concentrated sulfuric acid and hydrogen peroxide [30%] at a volume ratio of 7:3) for 10 min to remove trace contaminants on the gold electrodes of the sensor surface. Then the QCM sensors were washed three times alternately with ethanol and deionized water, and finally dried with high-purity nitrogen. The spraying process involved a volume of 300 μL , a nozzle size of 0.2 mm, and a distance of 18 cm between the spray pen nozzle and the substrate. Subsequently, the sprayed substrate was dried in a vacuum oven set at 60 °C for a duration of 6 h. Ultimately, the sensitive film coated QCM sensor was utilized for humidity detection.

2.4 | Characterization

The functional groups of GO, microgel, and GO/microgel materials were determined using a FTIR spectrometer

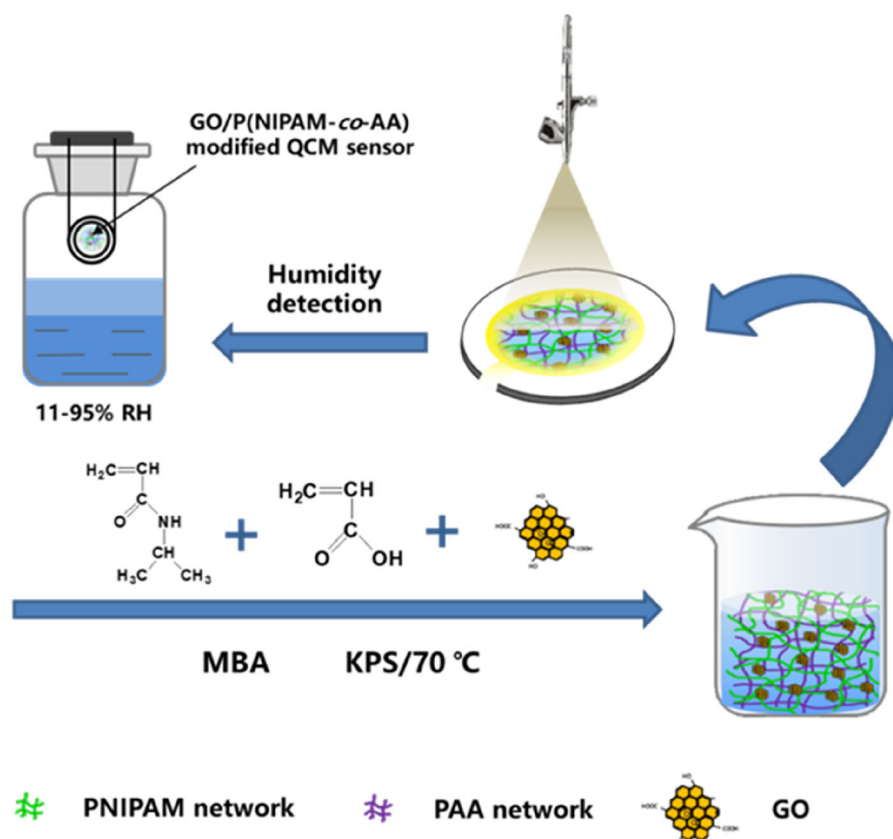


FIGURE 1 Preparation process of GO/P(NIPAM-co-AA) sensitive film modified quartz crystal microbalance sensor.

(Nicolet Avatar 370, Nicolet Instruments). The spectrum of the material was measured employing a UV-vis spectrophotometer (UV 1800, Shimadzu Corporation, Japan). The particle size was analyzed using a Nano-ZS analyzer (Malvern Instruments Ltd., UK). The sample's Raman spectra was characterized utilizing a DXR Raman spectrometer (Thermo Fisher Scientific, USA). The hydrophilicity and hydrophobicity of the materials were tested using a contact angle tester (Beijing Harke Testing Instrument Factory, HARKE-SPCA). Surface morphology was examined using a JSM-6360LA SEM (JEOL, Japan). The roughness was observed through laser scanning confocal microscope (LSCM, Mahr MarSurf CM, Mangofeld Technology Group). The application of this material in humidity sensing was analyzed with QCM (Suzhou Siju Biomaterials Co., Ltd., QCM-DBY).

3 | RESULTS AND DISCUSSION

3.1 | FTIR and UV-vis analysis

Comparing FTIR data can offer evidence of successful copolymerization and crosslinking, as depicted in Figure 2A. The spectra of GO/P(NIPAM-co-AA) reveal a broad absorption band associated with —OH at 3410 cm^{-1} and a C=O absorption band in GO at 1627 cm^{-1} .⁵⁹ A distinct peak

emerges at 1724 cm^{-1} , primarily belonging to stretching vibration of carboxyl (—COOH) groups from AA monomer units within P(NIPAM-co-AA) microgels. Additionally, the carbonyl stretching vibration (amide I) at 1650 cm^{-1} and the N—H bending vibration (amide II) at 1545 cm^{-1} arise from the functional groups of NIPAM monomer units. Hence, FTIR data confirms successful preparation of the composite microgels through in situ radical polymerization.

Figure 2B depicts the UV-vis spectra of GO, pure microgels, and composite microgels. Two distinct characteristic absorption peaks appear at 230 and 300 nm, corresponding to the $\pi\text{—}\pi^*$ and $n\text{—}\pi^*$ transitions of C=C bonds within the aromatic ring of GO.⁶⁰ Furthermore, the GO/P(NIPAM-co-AA) solution distinctly manifests varied absorption peak characteristics in the spectrum, suggesting the binding of GO with microgels of NIPAM and AA.

3.2 | Particle size analysis

The particle size distribution of P(NIPAM-co-AA) and GO/P(NIPAM-co-AA) composite microgels after polymerization with GO is illustrated in Figure 2C. According to Figure 2C, the average diameter data of pure microgels dispersed in water within 1000–2300 nm, with an average diameter of approximately 1525 nm. Following compounding with GO, the particle size distribution width band of the

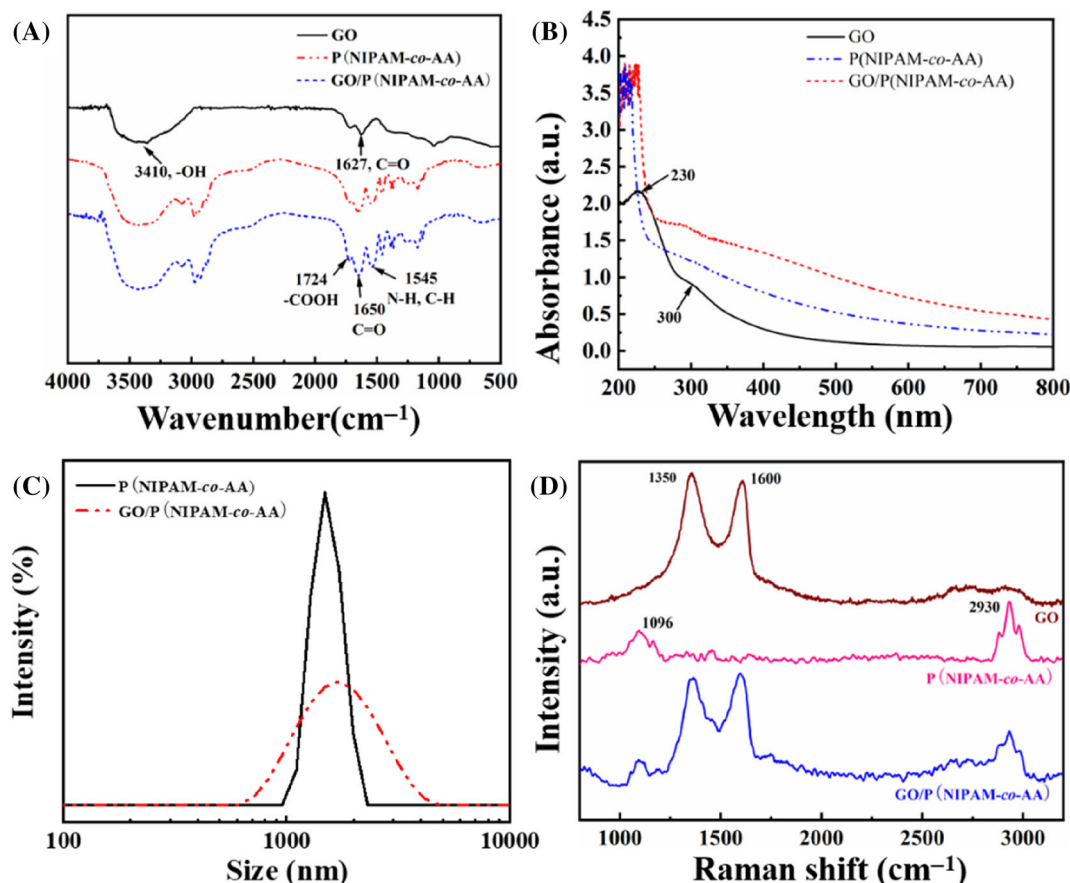


FIGURE 2 (A) Fourier transform infrared spectra, (B) UV-vis spectra, (C) particle size distribution, and (D) Raman spectra of GO, P(NIPAM-co-AA), and GO/P(NIPAM-co-AA) composite microgels.

microgel widened, resulting in an average diameter of about 1816 nm, which surpasses that of pure microgel. The significant difference in particle size between P (NIPAM-co-AA) and GO/P (NIPAM-co-AA) microgels is due to the binding of GO to the microgels. Note that the size of GO is in the range of 1–2 μm . It is supposed that the simple mixing of GO with microgels does not result in an increase in particle size of microgels. On the contrary, GO particles owing oxygen-containing groups and hydrophilic performance, are easily combined with monomer molecules during the polymerization process, and be wrapped into the interior of the microgel, resulting in an increase in the particle size of the microgel. In addition, compared with pure microgels, composite microgels can provide more adsorption sites for water molecules and rigid and hydrophilic GO component, which are conducive to the improvement of the frequency response of the QCM sensor.

3.3 | Raman spectroscopic analysis

Figure 2D depicts a Raman spectral comparison of GO, P(NIPAM-co-AA), and GO/P(NIPAM-co-AA) composite

microgels. From Raman spectrum of GO, two distinct characteristic peaks emerge around 1350 and 1600 cm^{-1} , corresponding to D and G peaks in GO. Notably, in the GO/P(NIPAM-co-AA) spectrum, both D and G peaks are evident, indicating the presence of GO within the composite microgels. Furthermore, prominent absorption peaks are observed at 1096 and 2930 cm^{-1} , likely stemming from stretching vibrations of C–C and C–H in P(NIPAM-co-AA) microgels.

3.4 | Contact angle analysis

The water contact angle images of GO, P(NIPAM-co-AA), and GO/P(NIPAM-co-AA) samples, along with their metallographic microscope photographs, are depicted in Figure 3. It can be observed that water contact angles on surfaces of GO, P(NIPAM-co-AA), and GO/P(NIPAM-co-AA) composite microgels are measured as 38.5°, 54.3°, and 37°, respectively. These angles are all less than 90°, indicating that these materials are hydrophilic and suitable for use in humidity sensors. Notably, the GO/P(NIPAM-co-AA) composite microgel exhibits a

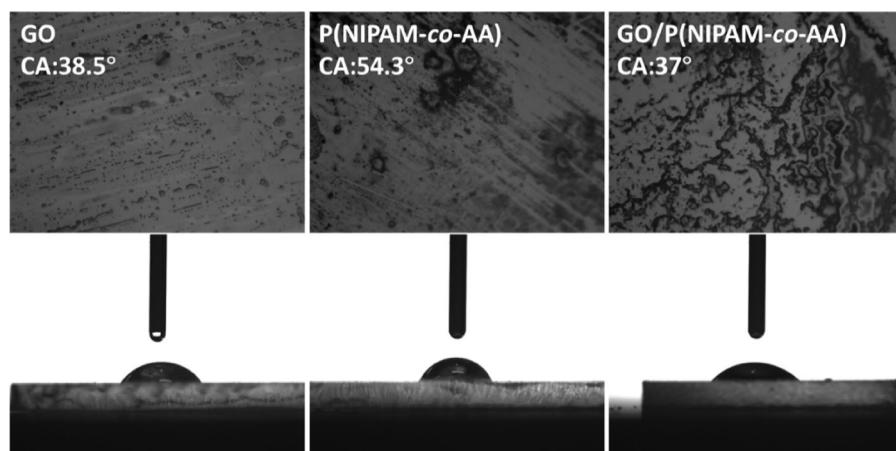


FIGURE 3 Water contact angles of GO, P(NIPAM-co-AA), and GO/P(NIPAM-co-AA) composite microgels.

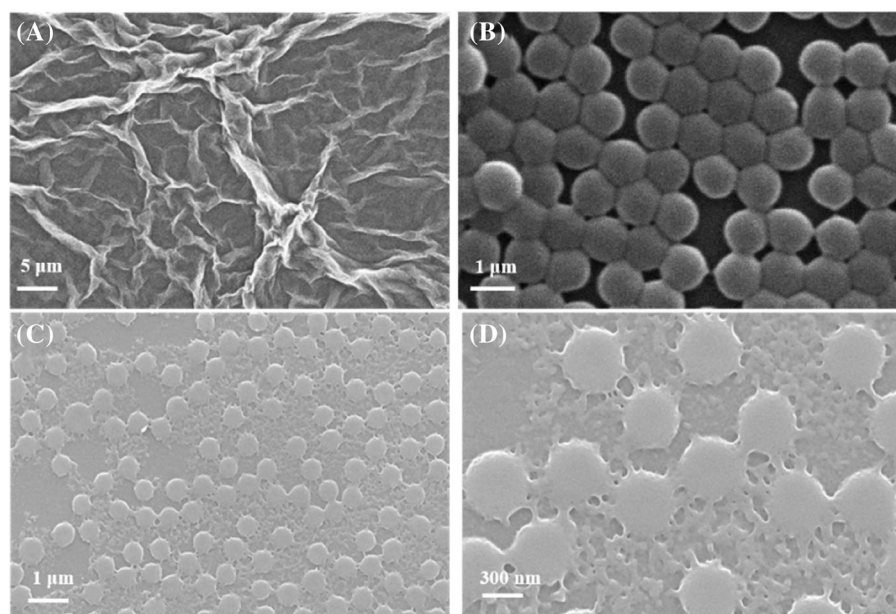


FIGURE 4 Scanning electron microscope images of (A) GO (5 μm), (B) P(NIPAM-co-AA) microgels (1 μm scale), and GO/P(NIPAM-co-AA) composite microgels at (C) 1 μm and (D) 300 nm scales.

smaller water contact angle and a rougher surface compared to the others, suggesting a stronger affinity for water molecules. This characteristic grants it an advantage in humidity sensor applications.

3.5 | Morphology and roughness analysis

The surface topography of GO, P(NIPAM-co-AA), and GO/P(NIPAM-co-AA) samples is depicted in Figure 4. The SEM image illustrates the wrinkling and folding topography of GO alongside the uniform spherical morphology of P(NIPAM-co-AA) microgels on a smooth substrate. In Figure 4C, the morphology of the microgel particles postbinding with GO is presented. It is evident that the composite microgel exhibits uniform sizing with a dry-state diameter of approximately 500 nm, which differs from its hydrated particle size as determined by

particle size analysis. Figure 4D provides a magnified view revealing that the film covering the substrate is coarser and possesses a larger specific surface area compared to pure microgels. This characteristic facilitates an increased availability of binding sites for water molecules, consequently enhancing the sensor's response rate.

To further determine the roughness of GO/P(NIPAM-co-AA) composite microgels, samples were scanned using laser scanning confocal microscopy (LSCM) for analytical imaging. Figure 5A1–A3 display microscope images of GO, P(NIPAM-co-AA), and GO/P(NIPAM-co-AA) samples, showcasing the excellent film-forming properties of the samples. Figure 5B1–B3 present their three-dimensional imaging maps, revealing roughness (R_a) values of 243, 108, and 441 nm for the three samples, respectively. The increased roughness observed for GO/P(NIPAM-co-AA) sample is based on the combination of GO and microgels. The LSCM data corroborates the findings of the SEM analysis.

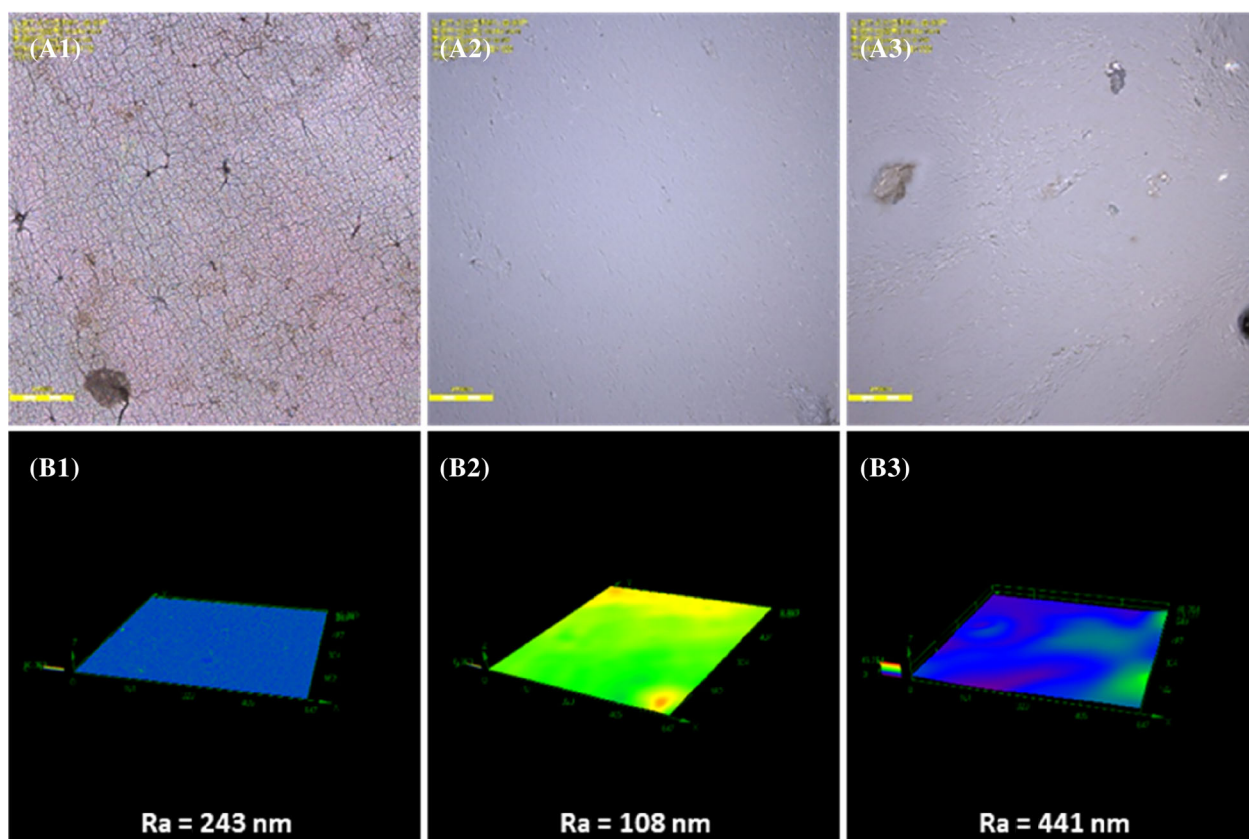


FIGURE 5 LSCM of (A1) GO, (A2) P(NIPAM-co-AA) microgels, (A3) GO/P(NIPAM-co-AA) composite microgels, and their corresponding (B1–B3) three-dimensional imaging maps.

3.6 | QCM dynamic response characteristics and sensing tests

First, we discuss the influence of the spray amount of sensitive materials on the performance of QCM sensors. Figure 6A displays the response curves of GO/P(NIPAM-co-AA) modified QCM sensors with varying spray volumes (100, 200, and 300 μL) within the range of 11%–95% RH, while Figure 6B illustrates the corresponding film thickness. As the deposited amount of GO/P(NIPAM-co-AA) microgel increases from 100 to 300 μL , the film thickness escalates from 1.50 to 1.97 μm . Since the amount of deposition on the surface of a QCM sensor increases, the more active sites can be provided, leading to a larger number of hydrophilic groups and a higher frequency response. The frequency response of GO/P(NIPAM-co-AA) modified QCM sensors amplifies with the increase in the spray amount of sensitive materials. However, when the spraying volume exceeds 300 μL , the oscillation of QCM sensor becomes very unstable or its inability even made the QCM sensor stop operating. Therefore, we selected the GO/P(NIPAM-co-AA) modified QCM sensor with the highest sensitivity (300 μL) for subsequent experiments.

Figure 7A illustrates the frequency responses of QCM humidity sensors utilizing various materials, including P(NIPAM-co-AA), GO, and GO/P(NIPAM-co-AA), upon reaching absorption equilibrium under varying humidity conditions. P(NIPAM-co-AA) microgels, with their large size, are abundant in hydrophilic groups, such as amide and carboxylic acid groups, facilitating effective water molecule binding. After binding to water molecules, P(NIPAM-co-AA) microgels coated on the QCM sensor surface alone become soft and hydrated, leading to highly viscoelastic properties and a mediocre frequency response. It is evident that the pure GO-modified QCM sensor exhibits a lower responsiveness to humidity compared with the pure P(NIPAM-co-AA) modified QCM sensor. This discrepancy arises from the tightly bound two-dimensional structure of GO to the sensor surface, lacking a three-dimensional configuration. Moreover, GO possesses a limited number of oxygen-containing groups primarily located at its edges, resulting in fewer active sites for water molecule binding. However, the combination of the two components, with GO as a rigid scaffold and microgels as functional and hydrophilic components, leads to a three-dimensional configuration, a certain rigid structure, abundant binding sites, and a highly sensing

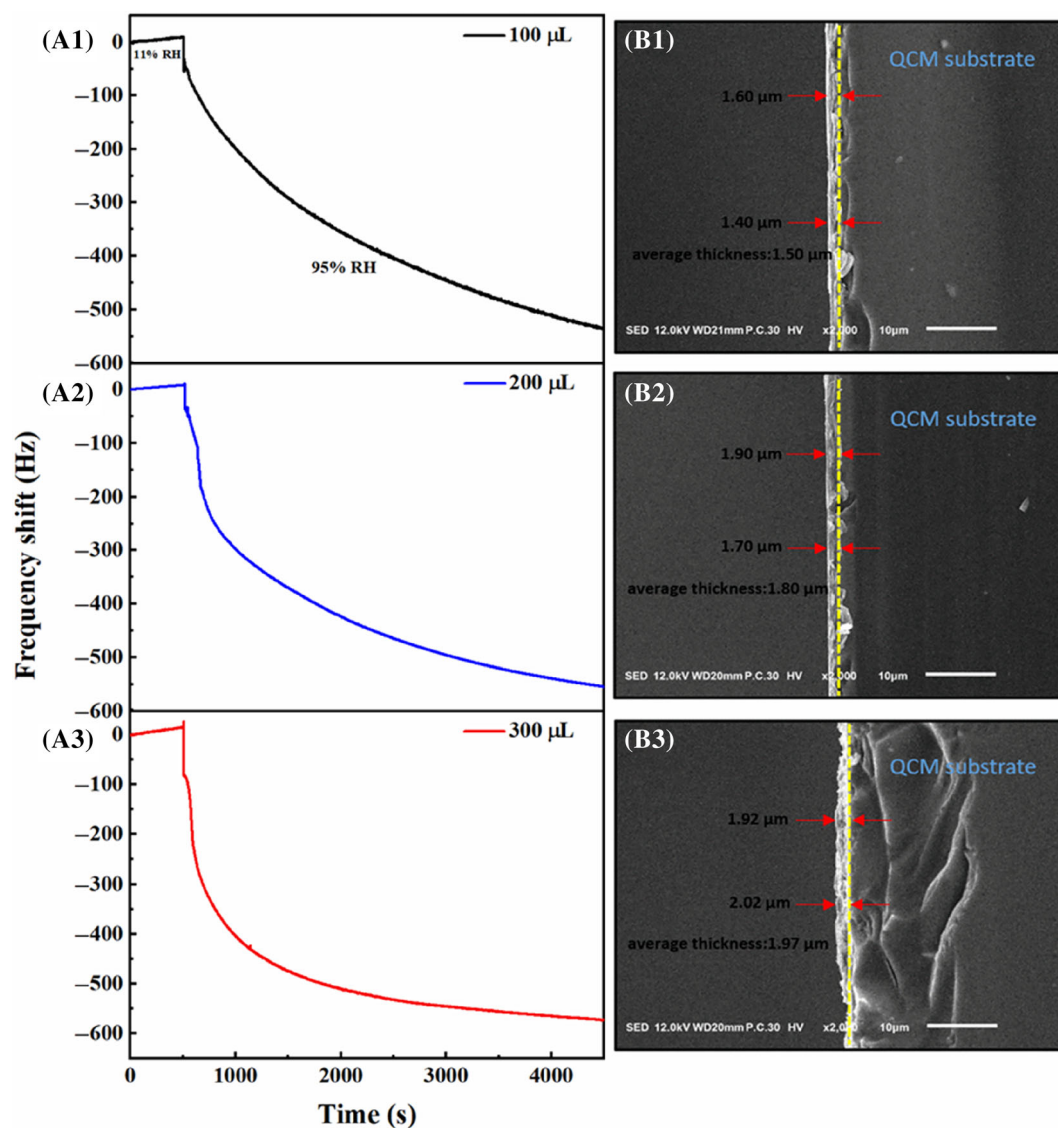


FIGURE 6 Real-time response curves of GO/P(NIPAM-*co*-AA) sensitive film-modified quartz crystal microbalance sensors with spray volumes of (A1) 100 μL , (A2) 200 μL , and (A3) 300 μL at 11%–95% RH humidity, and scanning electron microscope images corresponding to different film thicknesses at (B1) 100 μL , (B2) 200 μL , and (B3) 300 μL .

stability. As shown in Figure 7A, the frequency response of composite microgel modified QCM sensors has a significant increase in frequency shifts within 11%–95% RH, which is better than that of the QCM sensors modified with two materials including pure microgels and GO, separately, indicating the synergistic effect of GO and P(NIPAM-*co*-AA) microgels.

Furthermore, Figure 7B presents linear fitting curves indicating that all three QCM sensors employing different materials exhibit good linearity, with correlation coefficient (R_2) values of 0.99, 0.93, and 0.95, respectively. Notably, the sensitivity of QCM sensors utilizing GO/P(NIPAM-*co*-AA) material reaches 7.52 Hz/% RH.

The frequency response of a GO/P(NIPAM-*co*-AA) modified QCM sensor across varying humidity levels (11%–95% RH) is illustrated in Figure 7C. Initially, the

GO/P(NIPAM-*co*-AA) modified QCM sensor is exposed to an 11% RH environment, and the resonance frequency signal obtained serves as a reference line once the frequency stabilizes. Upon transitioning the modified QCM sensor to a 33% RH environment, the mass on its surface increases as the surface-sensitive film adsorbs water molecules, consequently reducing the frequency response of the QCM sensor. Initially, there is a rapid decreased Δf of the modified sensor, followed by a tendency to stabilize, indicating saturation of water molecules adsorbed by the GO/P(NIPAM-*co*-AA) under this humidity condition. Subsequently, when returning to an 11% RH environment, water molecules gradually desorb from the sensitive film due to the decreased relative humidity until reaching the initial state for complete desorption. This entire process constitutes a complete adsorption–desorption

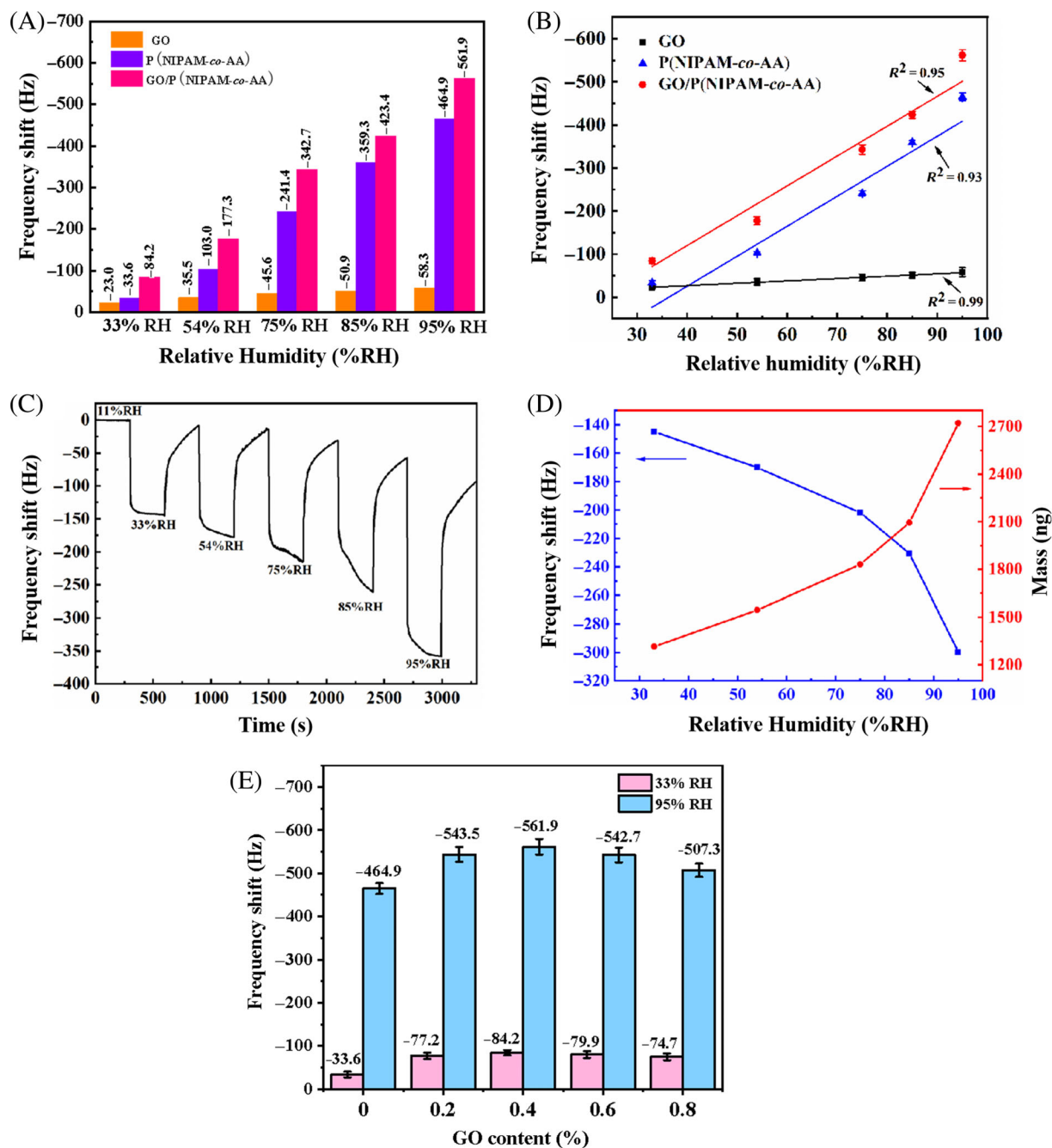


FIGURE 7 (A) Frequency shift of quartz crystal microbalance (QCM) humidity sensors modified with GO, P(NIPAM-co-AA), and GO/P(NIPAM-co-AA) materials under different humidity conditions; (B) Linear fitting curves of frequency response of QCM sensors modified by three materials under different humidity conditions; (C) Frequency response of GO/P(NIPAM-co-AA) modified QCM sensors 11%–95% RH; (D) Relationship between frequency response and mass change at different humidity (11%–95% RH); (E) Frequency responses of QCM humidity sensors modified with GO/P(NIPAM-co-AA) materials at different GO content (0.2 and 0.4, 0.6, 0.8 wt%) under low (33% RH) and high (95% RH) humidity conditions.

cycle, repeated for subsequent cycles. The alteration in mass of GO/P(NIPAM-co-AA) composites deposited on QCM sensors can be correlated with frequency shift using the Sauerbrey equation.²²

$$\Delta m = \frac{-C \Delta f_n}{n}, \quad (1)$$

where Δm represents the area mass density of the absorbing film (measured in unit area mass, ng cm^{-2}), C is $17.7 \text{ ng cm}^{-2} \text{ Hz}^{-1}$, Δf_n denotes the frequency shift of QCM sensor at harmonic number n (1, 3, 5, 7, ...), and the effective area of the blank QCM sensor is 1.54 cm^2 . Normally, the harmonic number was chosen to be 3. In Figure 7D, the change in frequency shift of the

GO/P(NIPAM-co-AA) modified QCM sensor and the mass change of water molecules absorbed at different humidities are depicted. As moisture levels increase, more water molecules adhere to the sensitive film, leading to increased mass change and a decreased frequency shift.

By changing the concentration of GO dispersion, GO composite microgels with different GO content (0 wt%, 0.2 wt%, 0.4 wt%, 0.6 wt%, and 0.8 wt%) can be obtained. The impact of supplementing GO content on the performance of QCM humidity sensors has been studied. Figure 7E shows frequency responses of QCM humidity sensors modified with GO/P(NIPAM-co-AA) materials at different GO content under low (33% RH) and high (95% RH) humidity conditions. From Figure 7E, with the increase of GO content from 0 to 0.4 wt%, the frequency response value of QCM sensors modified with GO/P(NIPAM-co-AA) was increased, indicating the introduction of GO as a rigid scaffold and its effective combination with microgels as functional and hydrophilic component. However, when the GO content was increased from 0.4 wt% to 0.8 wt%, the frequency response value of QCM sensors modified with GO/P(NIPAM-co-AA) was gradually decreased, indicating the decreased amount of active binding sites of GO/microgel film with water molecules. The humidity sensing mechanism of GO/P(NIPAM-co-AA) modified QCM sensors can be explained that the

combination of the two components, with GO as a rigid scaffold and microgels as functional and hydrophilic components, leads to a three-dimensional configuration, a certain rigid structure, abundant binding sites, and a highly sensing stability. The frequency response of composite microgel modified QCM sensors has a significant increase in frequency shifts within 11%–95% RH, which is better than that of the QCM sensors modified with two materials separately. Therefore, the enhanced sensor performance is due to synergistic effects between GO and P(NIPAM-co-AA) microgels at a suitable GO content of 0.4 wt%. The GO/P(NIPAM-co-AA) modified QCM sensors with 0.4 wt% GO were used for the following studies of repeatability, response-recovery time, hysteresis characteristics, and long-term stability.

3.7 | Repeatability of QCM humidity sensors

The repeatability curves of the modified QCM sensors at relative humidity levels between 11% and 95% are depicted in Figure 8. In Figure 8A, the P(NIPAM-co-AA) microgel-modified QCM humidity sensor exhibits poor repeatability. This observation may stem from the viscoelastic nature of the hydrophilic P(NIPAM-co-AA) microgel,

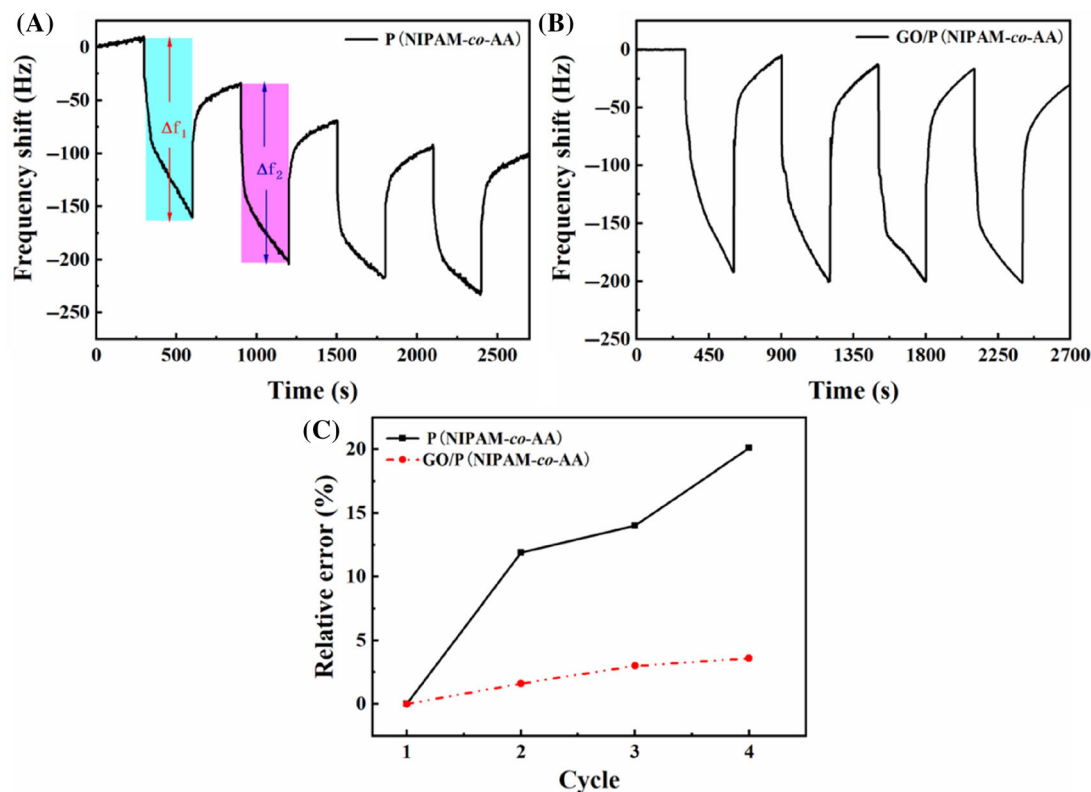


FIGURE 8 (A) Repeatability response curve of P(NIPAM-co-AA) modified quartz crystal microbalance (QCM) sensor in four cycles of 11%–95% RH; (B) Repeatability response curves of GO/P(NIPAM-co-AA) modified QCM sensor in four cycles of 11%–95% RH; (C) Relative error of QCM sensors modified with P(NIPAM-co-AA) and GO/P(NIPAM-co-AA) in each cycle.

which tends to be soft and moist, thereby leading to significant energy dissipation. Consequently, the vibration of the QCM sensor is adversely affected. Furthermore, the incorporation of GO with P(NIPAM-co-AA) microgels marginally mitigates discrepancies in repeatability, as illustrated in Figure 8B. To provide a more intuitive depiction of the error in each measurement cycle, the relative error is defined as per Equation (2).

$$\text{Relative error} = \left| \frac{\Delta f_1 - \Delta f_n}{\Delta f_1} \right| \times 100\%, \quad (2)$$

where Δf_1 and Δf_n are frequency shift in the first and n th ($n = 2, 3, 4, \dots$) test cycles, respectively. As shown in Figure 8C, the relative error of P(NIPAM-co-AA) modified QCM sensor is obviously becoming large as the cycle time increases. However, the relative error of GO/P(NIPAM-co-AA) modified QCM sensor is small, indicating that the sensor has excellent reversibility and repeatability.

3.8 | Response-recovery time, hysteresis characteristics, and long-term stability

Response time and recovery time serve as pivotal indicators for assessing the practicality of humidity

sensors. The time taken for the QCM sensor's response value to attain 90% of the full frequency shift is typically designated as the response time during adsorption or recovery time during desorption. As illustrated in Figure 9A, the response-recovery time of a GO/P(NIPAM-co-AA) based QCM humidity sensor reveals a response time of 44 s and a recovery time of 134 s within 11%–95% RH. These findings underscore the capability of the GO/P(NIPAM-co-AA) modified QCM sensor to swiftly adsorb and desorb water molecules. Microgels containing many hydrophilic groups including —OH, —COOH, and —CONH₂ groups, strong interactions are present between the structure of microgels and water molecules, making it difficult to desorb water molecules in a high humidity environment. Humidity hysteresis emerges as a crucial parameter for evaluating QCM humidity sensors. Specifically, this parameter denotes the lack of alignment between the sensor's response curves during the processes of water adsorption and desorption at various humidity levels. It can be quantified by calculating the ratio of the maximum difference in the adsorption and desorption response curves in comparison to the full-scale frequency change.

Figure 9B reveals that the QCM humidity sensor utilizing a P(NIPAM-co-AA) sensitive film exhibits a notable

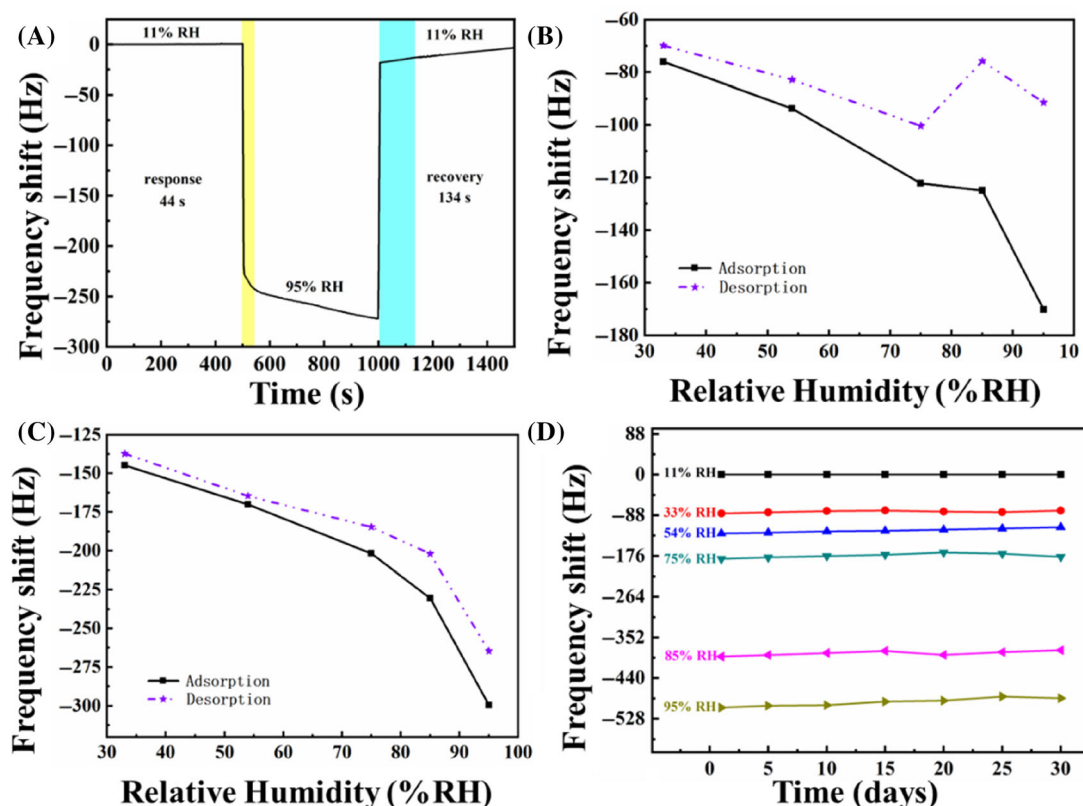


FIGURE 9 (A) Response-recovery curve of GO/P(NIPAM-co-AA) modified quartz crystal microbalance (QCM) sensors; Hysteresis curves of (B) P(NIPAM-co-AA) and (C) GO/P(NIPAM-co-AA) modified QCM sensors at 11%–95% RH; (D) Long-term stability of GO/P(NIPAM-co-AA) modified QCM humidity sensors.

disparity in response values between the adsorption and desorption processes, evident in the distinct deviation of the adsorption and desorption curves. However, Figure 9C illustrates that the GO/P(NIPAM-co-AA) modified QCM sensor demonstrates reduced hysteresis. While not achieving complete desorption, it proves more suitable for practical humidity measurement compared to the former P(NIPAM-co-AA) modified QCM sensor. It should be emphasized that the QCM sensor modified with the pure microgel shows increased humidity hysteresis, due to the viscoelastic and soft characteristics of the microgels. On the contrary, because of the introduction of rigid and hydrophilic GO, composite microgels have reduced moisture hysteresis than pure microgels.

The long-term stability of QCM humidity sensors employing GO/P(NIPAM-co-AA) sensitive film under various humidity conditions was examined. The GO/P(NIPAM-co-AA) modified QCM sensor underwent exposure to air for a month, with moisture sensitivity tests conducted every 5 days to measure the resonance frequency shift. From Figure 9D, Δf of the GO/P(NIPAM-co-AA) modified QCM humidity sensor exhibits minor fluctuations, ensuring commendable long-term stability and sensor quality.

4 | CONCLUSIONS

This study focuses on the synthesis of GO/P(NIPAM-co-AA) through in situ radical copolymerization. Through a comprehensive analysis including FTIR, UV-vis, DLS, and SEM, the composition, particle size, and morphology of the microgels were confirmed. A GO/P(NIPAM-co-AA) film was subsequently fabricated on a QCM sensor surface by spraying a mixture dispersion. To evaluate the surface hydrophilicity and roughness of the QCM sensors, comparisons were made among GO, P(NIPAM-co-AA) film, and GO/P(NIPAM-co-AA) composite film using water contact angle and LSCM. These analyses verified the advantages of GO/P(NIPAM-co-AA) for humidity sensor applications. QCM sensor equipped with a GO/P(NIPAM-co-AA) sensitive film exhibited significant responses in various humidity environments. Its sensitivity reached 7.52 Hz/% RH, with a response time of 44 s and a recovery time of 134 s. The sensor demonstrated repeatability and reversibility during testing. Moreover, the addition of GO notably improved the hysteresis of the QCM sensor compared to the pure P(NIPAM-co-AA) microgel-modified QCM sensor. In the future, the GO/microgel composite materials with functionalities can further be studied for revealing the interaction between materials and organic gas molecules and fabricating highly sensitive gas sensors.

ACKNOWLEDGMENTS

This project is supported by the National Natural Science Foundation of China (grant no. 21704008). Further financial support provided by the Postgraduate Research & Practice Innovation Program of Jiangsu Province is also gratefully acknowledged (grant no. KYCX23_3036).

CONFLICT OF INTEREST STATEMENT

The authors declare no conflict of interest.

DATA AVAILABILITY STATEMENT

The data that support the findings of this study are available from the corresponding author upon reasonable request.

ORCID

Zheng Cao  <https://orcid.org/0000-0003-2018-1569>

REFERENCES

- [1] J. Gubbi, R. Buyya, S. Marusic, M. Palaniswami, *Future Gener. Comput. Syst.* **2013**, 29, 1645.
- [2] Y. Wei, D. Liang, H. Zhou, S. Huang, W. Zhang, J. Gu, C. Hu, X. Lin, *Composites, Part A* **2022**, 153, 106739.
- [3] A. Iqbal, P. Sambyal, J. Kwon, M. Han, J. Hong, S. J. Kim, M.-K. Kim, Y. Gogotsi, C. M. Koo, *Compos. Sci. Technol.* **2021**, 213, 108878.
- [4] Z.-X. Wang, X.-S. Han, Z.-J. Zhou, W.-Y. Meng, X.-W. Han, S.-J. Wang, J.-W. Pu, *Compos. Sci. Technol.* **2021**, 213, 108931.
- [5] S. Kano, M. Fujii, *ACS Sustain. Chem. Eng.* **2018**, 6, 12217.
- [6] L. Wang, J. Xu, X. Wang, Z. Cheng, J. Xu, *Sens. Actuators, B* **2019**, 288, 289.
- [7] P. H. Phuoc, C. M. Hung, N. Van Toan, N. Van Duy, N. D. Hoa, N. van Hieu, *Sens. Actuators, A* **2020**, 303, 111722.
- [8] X. Zhao, Y. Long, T. Yang, J. Li, H. Zhu, *ACS Appl. Mater. Interfaces* **2017**, 9, 30171.
- [9] R. Zhou, J. Li, H. Jiang, H. Li, Y. Wang, D. Briand, M. Camara, G. Zhou, N. F. de Rooij, *Sens. Actuators, B* **2019**, 281, 212.
- [10] X. Zhang, Z. Zhai, J. Wang, X. Hao, Y. Sun, S. Yu, X. Lin, Y. Qin, C. Li, *ChemNanoMat* **2021**, 7, 1117.
- [11] Y. Dong, E. M. Akinoglu, H. Zhang, F. Maasoumi, J. Zhou, P. Mulvaney, *Adv. Funct. Mater.* **2019**, 29, 1904290.
- [12] H.-L. Liang, M. M. Bay, R. Vadrucchi, C. H. Barty-King, J. Peng, J. J. Baumberg, M. F. L. De Volder, S. Vignolini, *Nat. Commun.* **2018**, 9, 4632.
- [13] Y. P. Zhang, V. P. Chodavarapu, A. G. Kirk, M. P. Andrews, *Sens. Actuators, B* **2013**, 176, 692.
- [14] Z. Li, J. Wang, L. Dai, X. Sun, M. An, C. Duan, J. Li, Y. Ni, *ACS Appl. Mater. Interfaces* **2020**, 12, 55205.
- [15] P. Tian, X. Gao, G. Wen, L. Zhong, Z. Wang, Z. Guo, *J. Colloid Interface Sci.* **2018**, 532, 517.
- [16] Z. Zheng, N. Kim, W. S. Wong, J. T. W. Yeow, *Sens. Actuators, B* **2021**, 327, 128920.
- [17] Z. Zheng, C. Tang, J. T. W. Yeow, *Sens. Actuators, B* **2020**, 320, 128596.
- [18] D. Zhang, N. Luo, Z. Xue, Y.-L. Bai, J. Xu, *ACS Appl. Nano Mater.* **2022**, 5, 2147.

- [19] B. Du, D. Johannsmann, *Langmuir* **2004**, *20*, 2809.
- [20] M. Cui, Y. Duan, Y. Ma, K. W. A. Al-Shwafy, Y. Liu, X. Zhao, R. Huang, W. Qi, Z. He, R. Su, *Langmuir* **2020**, *36*, 4503.
- [21] C. Ma, H. Zhou, B. Wu, G. Zhang, *ACS Appl. Mater. Interfaces* **2011**, *3*, 455.
- [22] Z. Cao, J. Guo, X. Fan, J. Xu, Z. Fan, B. Du, *Sens. Actuators, B* **2011**, *157*, 34.
- [23] B. Chen, F. Wei, Z. Ma, Y. Peng, H. Guo, Y. Wang, S. Guan, J. Fu, C. Jing, J. Cheng, J. Xu, S. Liu, *J. Polym. Sci.* **2024**, *62*, 1588.
- [24] Z. Cao, T. Tsoufis, T. Svaldo-Lanero, A.-S. Duwez, P. Rudolf, K. Loos, *Biomacromolecules* **2013**, *14*, 3713.
- [25] Z. Cao, P. I. Gordiichuk, K. Loos, E. J. R. Sudhölter, L. C. P. M. de Smet, *Soft Matter* **2016**, *12*, 1496.
- [26] S. Braun, M. Santi, D. E. Demco, I. Litzen, J. Uecker, R. Fechete, J. J. Walkowiak, A. Pich, *J. Polym. Sci.* **2024**, *62*, 2301.
- [27] P. Qi, C. Zhao, R. Wang, T. Fei, T. Zhang, *IEEE Sens. J.* **2018**, *18*, 5278.
- [28] K. Tang, X. Chen, X. Ding, X. Yu, X. Yu, *ACS Appl. Nano Mater.* **2021**, *4*, 10810.
- [29] Q. Hong, L. Zhao, F. Lin, N. Tan, X. You, B. Lu, B. Huang, J. Lv, Y. Chen, L. Tang, *ACS Appl. Mater. Interfaces* **2023**, *15*, 58734.
- [30] X. Cha, F. Yu, Y. Fan, J. Chen, L. Wang, Q. Xiang, Z. Duan, J. Xu, *Sens. Actuators, B* **2018**, *263*, 436.
- [31] J. Xie, H. Wang, Y. Lin, Y. Zhou, Y. Wu, *Sens. Actuators, B* **2013**, *177*, 1083.
- [32] W. Yan, D. Zhang, X. Liu, X. Chen, C. Yang, Z. Kang, *ACS Appl. Mater. Interfaces* **2022**, *14*, 31343.
- [33] J. Dai, G. Xie, C. Chen, Y. Liu, H. Tai, Y. Jiang, Y. Su, *Appl. Phys. Lett.* **2024**, *124*, 053701.
- [34] Y. Li, W. Li, Z. Jin, X. Luo, G. Xie, H. Tai, Y. Jiang, Y. Yang, Y. Su, *Nano Energy* **2024**, *122*, 109291.
- [35] Q. Zhang, G. Xie, M. Duan, Y. Liu, Y. Cai, M. Xu, K. Zhao, H. Tai, Y. Jiang, Y. Su, *ACS Appl. Nano Mater.* **2023**, *6*, 17445.
- [36] Y. Su, S. Chen, B. Liu, H. Lu, X. Luo, C. Chen, W. Li, Y. Long, H. Tai, G. Xie, Y. Jiang, *Mater. Today Phys.* **2023**, *30*, 100951.
- [37] C. Chen, G. Xie, J. Dai, W. Li, Y. Cai, J. Li, Q. Zhang, H. Tai, Y. Jiang, Y. Su, *Nano Energy* **2023**, *116*, 108788.
- [38] H. Pan, G. Chen, Y. Chen, A. Di Carlo, M. A. Mayer, S. Shen, C. Chen, W. Li, S. Subramaniam, H. Huang, H. Tai, Y. Jiang, G. Xie, Y. Su, J. Chen, *Biosens. Bioelectron.* **2023**, *222*, 114999.
- [39] P. Qi, Z. Xu, T. Zhang, *Chemosensors* **2022**, *10*, 522.
- [40] Z. Yuan, H. Tai, Z. Ye, C. Liu, G. Xie, X. Du, Y. Jiang, *Sens. Actuators, B* **2016**, *234*, 145.
- [41] Z. Wu, S. Zhu, X. Dong, Y. Yao, Y. Guo, S. Gu, Z. Zhou, *Anal. Chim. Acta* **2019**, *1080*, 178.
- [42] Y. Yao, X. Chen, X. Li, X. Chen, N. Li, *Sens. Actuators, B* **2014**, *191*, 779.
- [43] X. Leng, D. Luo, Z. Xu, F. Wang, *Sens. Actuators, B* **2018**, *257*, 372.
- [44] X. Ding, X. Chen, X. Chen, X. Zhao, N. Li, *Sens. Actuators, B* **2018**, *266*, 534.
- [45] Z. Cao, Y. Zhang, Z. Luo, W. Li, T. Fu, W. Qiu, Z. Lai, J. Cheng, H. Yang, W. Ma, C. Liu, L. C. P. M. de Smet, *Langmuir* **2021**, *37*, 12148.
- [46] Z. Cao, B. Du, T. Chen, J. Nie, J. Xu, Z. Fan, *Langmuir* **2008**, *24*, 12771.
- [47] T. Chen, Z. Cao, X. Guo, J. Nie, J. Xu, Z. Fan, B. Du, *Polymer* **2011**, *52*, 172.
- [48] Z. Cao, Y. Hu, Q. Yu, Y. Lu, D. Wu, A. Zhou, W. Ma, Y. Xia, C. Liu, K. Loos, *Adv. Eng. Mater.* **2017**, *19*, 1600826.
- [49] Z. Cao, T.-Y. Chen, X.-L. Guo, X.-J. Zhou, J.-J. Nie, J.-T. Xu, Z.-Q. Fan, B.-Y. Du, *Chin. J. Polym. Sci.* **2011**, *29*, 439.
- [50] H. Masoud, A. Alexeev, *ACS Nano* **2012**, *6*, 212.
- [51] R. Borrmann, V. Palchyk, A. Pich, M. Rueping, *ACS Catal.* **2018**, *8*, 7991.
- [52] B. P. Tripathi, N. C. Dubey, M. Stamm, *ACS Appl. Mater. Interfaces* **2014**, *6*, 17702.
- [53] Z. Cao, Y. Chen, Q. Zhang, Y. Xia, G. Liu, D. Wu, W. Ma, J. Cheng, C. Liu, *Nano* **2017**, *3*, 16.
- [54] Y. Wu, Y. Zhang, K. Wang, Z. Luo, Z. Xue, H. Gao, Z. Cao, J. Cheng, C. Liu, L. Zhang, *ACS Omega* **2021**, *6*, 5764.
- [55] G. Liu, C. Liu, Y. Chen, S. Qin, S. Yang, D. Wu, H. Xi, Z. Cao, *Nanosci. Nanotechnol. Asia* **2019**, *9*, 267.
- [56] X. Zhou, J. Nie, B. Du, *ACS Appl. Mater. Interfaces* **2017**, *9*, 20913.
- [57] X. Zhou, J. Nie, B. Du, *ACS Appl. Mater. Interfaces* **2015**, *7*, 21966.
- [58] M. H. Smith, L. A. Lyon, *Macromolecules* **2011**, *44*, 8154.
- [59] S. Rattana, N. Chaiyakun, N. Witit-anun, P. Nuntawong, S. Chindaudom, C. Oaew, P. L. Kedkeaw, *Procedia Eng.* **2012**, *32*, 759.
- [60] H. M. Hegab, Y. Wimalasiri, M. Ginic-Markovic, L. Zou, *Desalination* **2015**, *365*, 99.

How to cite this article: L. Ji, Y. Pan, Z. Cao, R. Wang, H. Yang, J. Cheng, C. Liu, X. Lu, L. C. P. M. de Smet, *J. Polym. Sci.* **2024**, *1*. <https://doi.org/10.1002/pol.20240504>